Australian Government
Department of Defence
Science and Technology

Flow Visualisation Around a Hemispherical Protuberance in the DST Group Water Tunnel

André Franck Bauer[1], *Jesse McCarthy*[2] *and Matteo Giacobello*[2]

[1] **School of Aerospace, Mechanical and Mechatronic Engineering, University of Sydney**
[2] **Aerospace Division**
Defence Science and Technology Group

DST-Group–TR–3482

ABSTRACT

The flow structures around a hemispherical protuberance were studied using dye-injection flow visualisation in the DST Group Water Tunnel. A 100 mm diameter hemisphere was placed in a laminar oncoming boundary layer, and video imaging of the dye streamlines were captured at diameter-based Reynolds numbers of 6.91×10^3 and 1.15×10^4. The observations generally agree well with previous studies, while analysis of the video footage has provided additional insight into the evolution of the unsteady flow field.

RELEASE LIMITATION

Approved for Public Release

Produced by

Aerospace Division
506 Lorimer St,
Fishermans Bend, Victoria 3207, Australia

Telephone: 1300 333 362

April, 2018
AR-017-170

APPROVED FOR PUBLIC RELEASE

Flow Visualisation Around a Hemispherical Protuberance in the DST Group Water Tunnel

Executive Summary

Aircraft are often fitted with external sensors housed in hemispherical shrouds, which alter the flow-field characteristics in their proximity. The impact on the local flow field could negatively affect the flight envelope and performance characteristics of the aircraft, yet there are relatively few qualitative experimental studies with clear, documented imagery of the flow structures around hemispherical protuberances. This is primarily due to the fact that most previous flow visualisation is quite dated and was subject to imaging and hardware limitations, thus sharp images were difficult to reproduce. This work is therefore done to provide more detailed imagery and updated observations on these hemisphere induced flow fields.

This study was conducted in the Defence Science and Technology (DST) Group Water Tunnel and involved dye injection around a 100 mm diameter hemispherical protuberance mounted on a flat plate ground plane, at diameter based Reynolds numbers of 6.91×10^3 and 1.15×10^4. An oncoming laminar boundary layer was allowed to naturally develop, partially immersing the hemisphere. Video imagery were obtained from two orthogonal perspectives that were spatially and temporally aligned. This allowed for clearer interpretation of the three-dimensional flow structures from the two orthogonal views.

Interpretation of the video footage has revealed additional detail regarding previously described phenomena in literature. This includes the formation and evolution of ‘hairpin’ vortices from the hemisphere lee-side as well as the periodic oscillation of the ‘horseshoe’ vortex system upstream of the hemisphere. Large-scale oscillations in the wake were also observed to occur for both Reynolds numbers, which indicated a possible mix of von Kármán vortex shedding and shear layer roll up over the hemisphere. The formation Strouhal number of the highlighted flow structures were estimated using the video footage; it was found that as Reynolds number increased, the Strouhal number of shear layer roll up increased, while the large-scale wake oscillations showed a small reduction in Strouhal number.

This page is intentionally blank

Contents

Figures

Tables

Glossary

DST	Defence Science and Technology
LED	Light Emitting Diode
RMS	Root-Mean-Square

Notation

D	Hemisphere diameter (mm)
f	Frequency (Hz)
H	Hemisphere height (mm)
Re_x	Reynolds number based on dimension x, $Re_x = \dfrac{U_\infty x}{\nu}$
Re_D	Reynolds number based on diameter D, $Re_D = \dfrac{U_\infty D}{\nu}$
St_D	Strouhal number based on diameter D, $St_D = \dfrac{fD}{U_\infty}$
U_∞	Free-stream flow speed (m/s)
x, y, z	Cartesian coordinates

Greek Symbols

δ	Laminar boundary layer thickness (mm)
ν	Kinematic viscosity (m^2/s)
θ	Stream-wise angular position along hemisphere meridian (°)

This page is intentionally blank

1. Introduction

1.1. Literature Review

The flow field produced by a surface mounted hemisphere (or hemispherical protuberance) is complex and has been the subject of a range of qualitative and quantitative investigations. Hemispherical protuberances are commonly found on aircraft in the form of external sensor shrouds. The presence of these protuberances could cause oscillations in the local flow field and/or structural vibrations, and hence could alter the dynamic characteristics of the aircraft. It is therefore important to understand the unsteady flow field surrounding a hemispherical protuberance.

Early work in understanding the flow surrounding surface mounted hemispheres was often limited to qualitative flow-visualisation studies. Researchers such as [1] conducted extensive analyses of the flow patterns induced both upstream and downstream of a hemispherical protuberance. Using hydrogen-bubble wires and dye visualisation in a water tunnel, they were able to elicit the formation of a steady vortex generated below the hemisphere upstream stagnation point, which displayed the same vorticity sense as the oncoming boundary layer (i.e. the 'Standing vortex' in Fig. 1). This vortex curves around the hemisphere and extends into the wake, forming a structure which has been described as a 'horseshoe' or 'necklace' vortex [1, 2]. Further detail was provided by [3] who observed that this vortex was actually a complex system of counter rotating vortex pairs that coalesce downstream to form the horseshoe shape. The evolution of these vortices is dependent on the boundary-layer thickness, state, and free-stream turbulence intensity [4].

The downstream flow can be categorised into a near-wake separated region and an unsteady vortex shedding region [1]. Flow separation off the hemisphere results in the formation of a recirculation zone immediately behind the hemisphere, the length of which has been shown to be dependent on upstream turbulence intensity [3]. There is a complex interaction between the separated shear layer and the outer flow which results in the periodic build-up and shedding of loop shaped vortices [1]. It was also reported that generation of these vortices from the shear layer is hard to visualise and further work is required to understand the finer detail of the flow structure at these points [5]. The shape of the loops has led many researchers to refer to them as 'hairpin' vortices. They consist of two counter rotating legs which originate close to the ground plane and angle upwards until they come together to form a loop or 'head'. There is vorticity in both the span-wise and stream-wise directions, which entrains surrounding fluid and results in the creation of secondary vortices as the entrained fluid is swept up by the velocity gradient in the boundary layer [1]. A hairpin vortex structure is shown in Fig. 1.

The evolution of hairpin structures in the wake has been extensively described by [1]. The dominant behaviour is vortex stretching, where parts of a single hairpin are accelerated in the stream-wise direction by the boundary layer velocity gradient; this leads to coalescence of multiple downstream hairpin legs. It was noted elsewhere that by varying the Reynolds number, the coalesence of multiple hairpin heads is affected significantly [5]. Here, the diameter based Reynolds number Re_D is defined as[1];

[1]It should be noted that some researchers have used a hemisphere radius based Reynolds number.

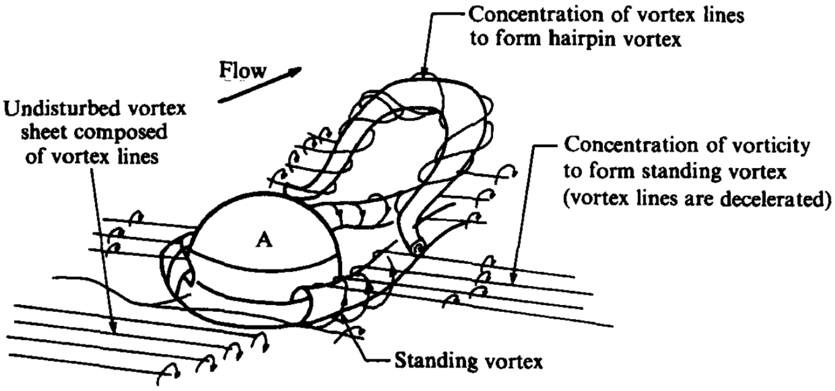

Figure 1: Vortex lines around a hemispherical protuberance as described by [1].

$$Re_D = \frac{U_\infty D}{\nu}, \tag{1}$$

where U_∞ is the free-stream flow speed, D is the diameter and ν is the fluid kinematic viscosity. It was observed by [5] that as Reynolds number increases, the distance between subsequent hairpin vortices decreases, which results in stronger interactions between subsequent vortices. It was also suggested that the three-dimensionality of the flow and the high levels of turbulence in the wake means that hairpin vortices do not persist far downstream [6]. Some elements of the flow pattern are similar to the wake behind a sphere or hemisphere in a laminar free-stream flow [7, 8], but in the presence of an oncoming boundary layer as opposed to a uniform flow, the evolution of hairpin vortex shedding is markedly different.

Owing to the downstream translation and periodicity of the vortices, there are significant oscillations in pressure distribution on the ground plane and the hemisphere [9]. Many researchers have used pressure tapped hemispheres and ground planes to quantify these distributions and the frequencies at which they occur [10, 11]. It was found in preliminary wind-tunnel tests of a hemisphere conducted at DST that at $Re_D = 6.36 \times 10^4$ the mean flow is symmetric across the stream-wise centre-line plane, while at $Re_D = 1.25 \times 10^5$ a noticeable asymmetry had developed due to the transitional nature of the flow on the windward side of the hemisphere. This is qualitatively consistent with previous work on flows around a circular cylinder by [12], who found that at a Reynolds number of about 3.4×10^5 the wake would become asymmetric in the mean. No pattern in the direction of the asymmetry was reported but hysteresis was detected. However, the study in [12] reported a tunnel blockage of about 20% and identified that the reported Reynolds numbers may not have been accurate.

In the flow regime where periodical vortex shedding is present, the dominant Strouhal number has been variously quantified to be between 0.1 and 0.5 [13, 14, 15, 16], and an increasing trend is apparent as Reynolds number increases [5]. Strouhal number, which is a form of non-dimensionalised frequency, is defined as;

$$St_D = \frac{fD}{U_\infty}, \tag{2}$$

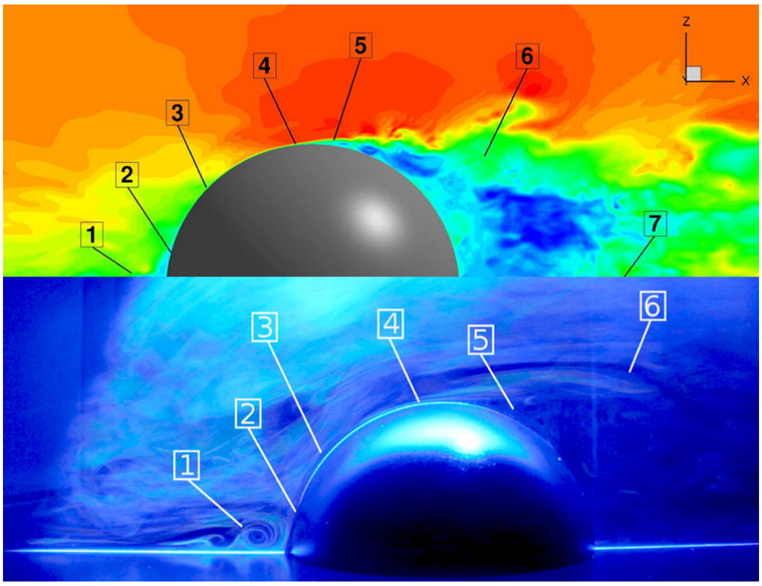

Figure 2: Computational (top) and experimental (bottom) flow visualisations around a hemispherical protuberance [4].

where f is frequency. It was reported by [17] that there is a correlation between the surface pressure fluctuations near the upstream stagnation point on the hemisphere and those around the downstream separated region.

A number of computational analyses have also been completed for hemispherical protuberances, with the results largely in qualitative agreement with experimental evidence. Detailed images outlining the primary horseshoe and hairpin structures, as well as secondary vortices generated from low momentum fluid entrainment in the wake, were provided in [18]. A number of researchers have conducted combined computational and experimental analyses, which have demonstrated broad agreement between simulated and flow visualisation results as in Fig. 2. This agreement is highly dependent on the fidelity of the computational model [4, 19, 20]. In [21], the analyses were expanded to include turret shaped protuberances and showed that the salient flow features are very similar to a standard hemisphere shape.

The large-scale flow pattern is generally understood and has been documented in many studies, but some ambiguity remains in understanding the finer details surrounding the generation of hairpin vortices and the interaction between the near-wake, shear layer and outer flow field. In particular there seems to be two main vortex shedding modes in the near wake, corresponding to the separated shear layer over the top of the hemisphere and the classical von Kármán shedding around the sides of the hemisphere [4]. There is also evidence of aperiodic switching between symmetric and anti-symmetric Kármán shedding types at the sides of the hemisphere; it was inferred in [19] that the dominant shedding type is dependent on small-scale turbulent structures. Nevertheless, the interaction between the shear layer roll up and the von Kármán type shedding requires further investigation.

There are significant disparities in flow conditions between studies in literature. Work has been conducted with the hemispherical protuberance fully or partially immersed in both turbulent and laminar boundary layers at a wide range of Reynolds numbers. Repeatability and reproducing the specific conditions from earlier work is challenging owing to the frequent use of a natural boundary layer developed along the test section of specific flow testing facilities. Despite these (and other) disparities, similar flow features have been reported. It is interesting to note that even with the hemisphere only partially immersed in a boundary layer as in [13], the mean flow patterns are qualitatively similar to those studies with full boundary layer immersion [4]. Still, it is difficult to draw direct quantitative comparisons between studies because the unsteady flow parameters are sensitive to the oncoming boundary layer and outer flow characteristics.

1.2. Objectives

The objectives of the dye-injection flow visualisation study conducted in the DST Group Water Tunnel are as follows:

- Add to the existing knowledge regarding the formation and evolution of horseshoe and hairpin vortices, using modern camera technology. Particular care was given to the placement of dye injection ports to ensure the near-wake region was visible and that the initial roll up of vorticity was captured.

- Capture video imagery of sufficient quality to provide a visual estimate of vortex shedding frequencies. Most of the previous work in this area predates digital video technology and the quality of the images in literature needs improvement if further flow details are to be identified.

- Identify areas of interest in the flow such that further quantitative studies could be better targeted and aid in the interpretation of this data.

2. Experimental Method

2.1. Water Tunnel

The DST Water Tunnel is a recirculating closed-circuit tunnel with a test section 380 mm wide, 510 mm deep and 1630 mm long. The test section is horizontally oriented with a free water surface and contains tempered glass walls to allow for flow visualisation. A 3.7 kW pump is capable of producing test section flow speeds of up to 0.6 m/s using a contraction ratio of 6:1 and a flow rate of approximately 3400 L/min. Inside the settling chamber there are a number of flow conditioning screens including a perforated stainless-steel plate, two fibreglass screens, and a honeycomb flow straightener. The turbulence intensity in the test section is less than 1% RMS, while the velocity varies less than 2% about the average and the flow angularity is less than $\pm 1.0°$ in both pitch and yaw angle [23]. In addition to the glass test section, there is also a glass window on the downstream wall of the diffuser. This facilitates upstream viewing in the cross-flow plane without mirrors as well as providing a suitable angle from which to light the test section. A full schematic of the water tunnel can be seen in Fig. 3.

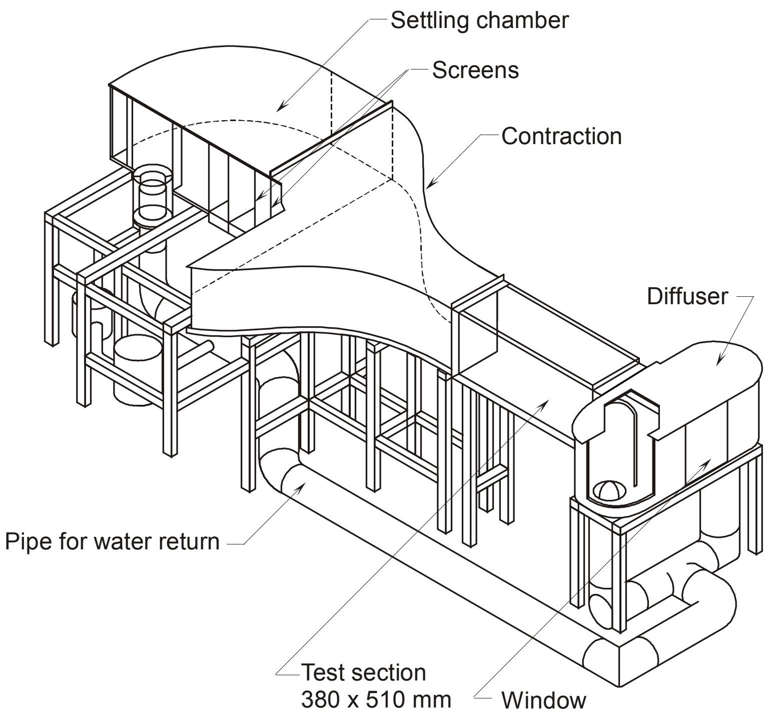

Figure 3: The DST Group Water Tunnel as depicted in [22].

The tunnel is fitted with six, air pressurised dye canisters that can be connected with plastic tubing to the desired location within the test section. This system allows for continuous injection of up to six dye colours. The manufacturer suggests that the optimal free stream velocity for dye flow visualisation studies is between 0.1 m/s and 0.15 m/s [23]. The dye injection rate can be controlled manually with flow rates ranging from 0 to 100 ml/s.

2.2. Test Articles

An elevated ground plane with a 6:1 elliptical leading edge was installed in the water tunnel to allow for the formation of a laminar boundary layer along its surface. A hemispherical protuberance of 100 mm diameter was placed with its apex 500 mm downstream of the ground plane leading edge. Thirty-two dye injection ports of 1 mm internal diameter were installed around the hemisphere as per Fig. 4. The ground plane also included a trailing edge flap that could be used to adjust the stream-wise pressure gradient and thus reduce the likelihood of any leading edge boundary layer separation. However, as discussed in Section 2.4, it was found that the trailing edge flap was not required for these tests.

The dye injection ports were positioned to enable injection close to the expected points of vorticity generation, making the flow structure visible as suggested by [24]. The circular pattern of ports allowed for injection near the horseshoe vortex system and the upstream separation point of the hemisphere. Additionally, the downstream array allows for injection in the near-wake or separated region where initial shear layer roll up occurs. A schematic of the dye port numbering system is shown in Fig. 5. The coordinate system shown is used throughout this report, with the x-axis lying on the stream-wise plane of symmetry and pointing directly

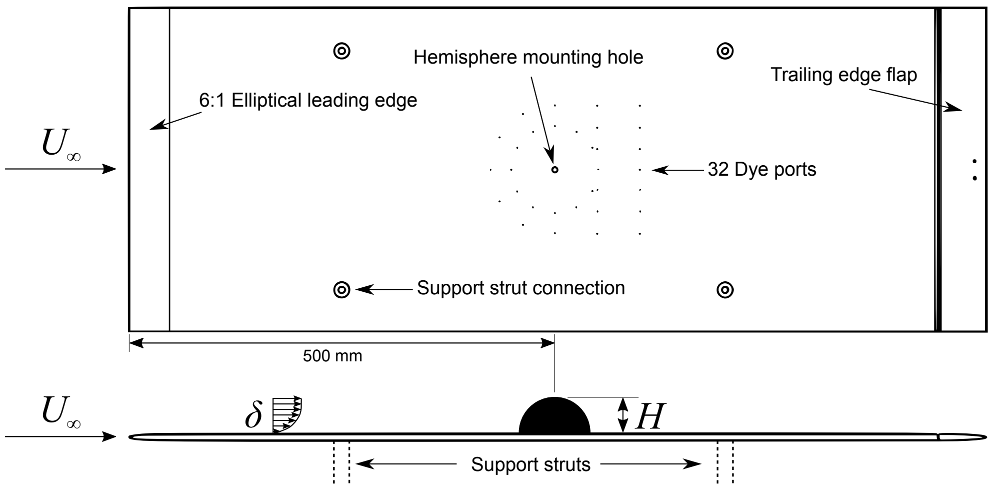

Figure 4: Diagram of the elevated ground plane with experimental parameters. Note that the schematic is not to scale.

downstream. A preliminary study was undertaken which explored dye injection from a range of port combinations. From this, port combinations that most clearly elicited the key expected flow features were established.

To avoid any potential free surface interaction and to provide better visibility, the ground plane was mounted upside-down in the tunnel. This also provided easy access to the injection ports and allowed for imaging through the glass surface on the bottom of the tunnel. As the dye is neutrally buoyant, gravity effects were considered negligible. It was also ensured that the hemisphere was positioned away from the tunnel-wall boundary layers. The full experimental installation in the water tunnel is shown in Fig. 6.

2.3. Test Conditions

Dye injections were conducted at nominal free-stream velocities of 0.06 m/s and 0.1 m/s with a water temperature of 26.2 ± 0.1 °C. At this temperature the kinematic viscosity of water was taken to be 8.68×10^{-7} m^2/s. Based on the hemisphere diameter, the Reynolds numbers tested were 6.91×10^3 and 1.15×10^4 according to Eq. (1). The hemisphere, ground plane and support geometry were estimated to give a test section blockage of 7.3%, and given that this value was only marginally greater the recommended value of 7% for incompressible flows [25], no corrections to Reynolds number were deemed necessary.

2.4. Oncoming Boundary Layer

A laminar boundary layer was allowed to form naturally on the elevated ground plane until it partially immersed the hemisphere. The boundary layer thickness δ was calculated using the flat plate Blasius solution;

$$\delta = \frac{4.9x}{\sqrt{Re_x}}, \tag{3}$$

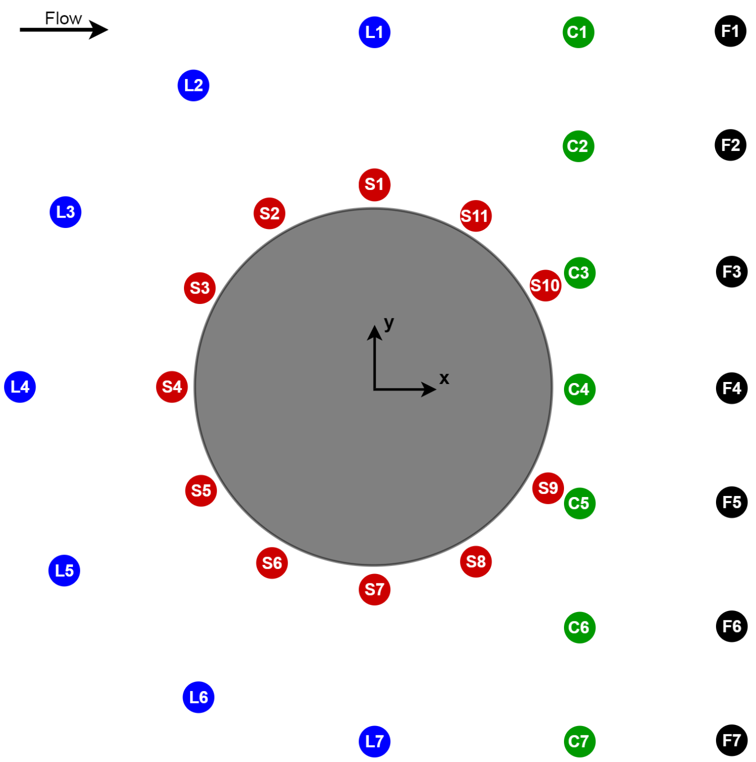

Figure 5: Dye injection port locations and designations. This diagram is not to scale.

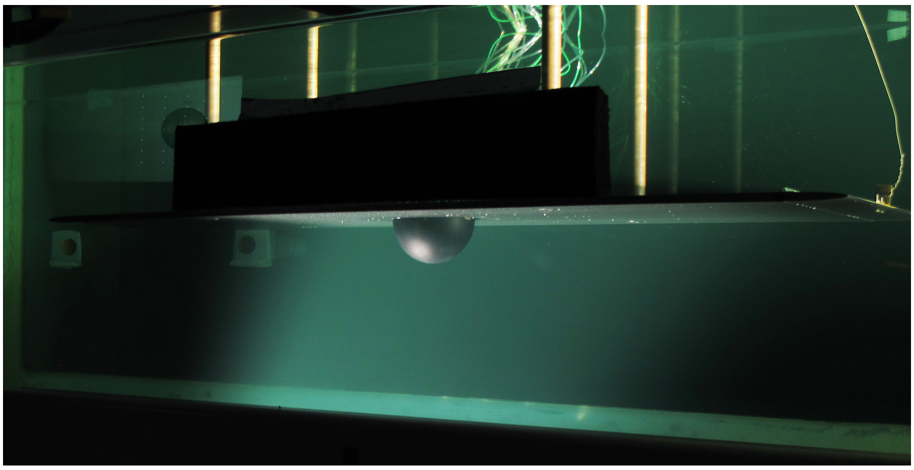

Figure 6: Hemisphere and ground plane installed in the DST Water Tunnel. The free-stream flow is from left to right.

where x is the distance from the flat plate leading edge and Re_x is the Reynolds number based on dimension x. Previous work in the DST Water Tunnel showed that the experimentally determined boundary layer thickness along a similar ground plane agreed very well with the Blasius solution [26]. Given free-stream velocities of 0.06 m/s and 0.1 m/s as well as the 500 mm distance between the ground plane leading edge and the hemisphere apex, the boundary layer thickness non-dimensionalised by the hemisphere height H was estimated to be 0.268 and 0.208 respectively. Preliminary visualisation of the impinging flow on the ground plane showed that there was no leading edge separation occurring, thus deflection of the trailing edge flap was not necessary for the duration of the tests.

2.5. Imaging Setup

Video footage of the experiment were acquired using two identical Sony HXR-NX series video cameras located underneath and to the side of the tunnel. Footage was recorded from two orthogonal planes, providing a top view (planar) and side view (cross-section) of the hemisphere and wake region. Higher shutter speeds were also used so as to avoid smearing, or time-averaging, of the dye motion. The cameras supported a time-code in/out feature to ensure that video recorded from both perspectives was synchronised. Thus, a single record instruction could be sent to simultaneously trigger both cameras, to ensure *in situ* temporal alignment of the video imagery. Also, both cameras were spatially aligned such that both perspectives could be directly compared. Post processing of the video imagery was then performed to place both perspectives in a single frame, and enhance the colours and contrast where necessary.

Diffuse lighting sources were placed around the tunnel to provide illumination for the dye. To ensure a high contrast of the dye, the plexiglass ground plane was painted matte black, the aluminium hemisphere was anodised black and a black curtain was positioned over the tunnel far-side window. However, the anodised coating on the hemisphere began to deteriorate as testing progressed, giving the hemisphere a dull colouring in the video footage, but the dye streak-lines could still be discerned effectively. A photograph of the experimental setup including cameras and lighting is shown in Fig. 7. Additionally, the image recording parameters are outlined in Table 1.

Additional video imagery were captured using a thin sheet of white light to illuminate only a stream-wise cross-section of the flow. This was found to be most effective when studying the $x - z$ plane along the centre-line. It was found that the light sheet clarified the formation and evolution of horseshoe vortices. A digital projector was used to generate the light sheet from underneath the tunnel and a 45° plane mirror was used to reflect the light 90° such that it illuminated the desired cross-section. This method was found to be highly effective, but produced relatively low illumination. Consequently, only the cross-section camera was used and it was moved closer to the tunnel, reducing the required zoom and enabling a wider aperture. This experimental setup is shown in Fig. 8.

Table 1: Image recording parameters for both cameras.

Parameter	Value
Resolution	1280 × 720 pixels
Shutter speed	1/100 s
Frame rate	50 frames/s

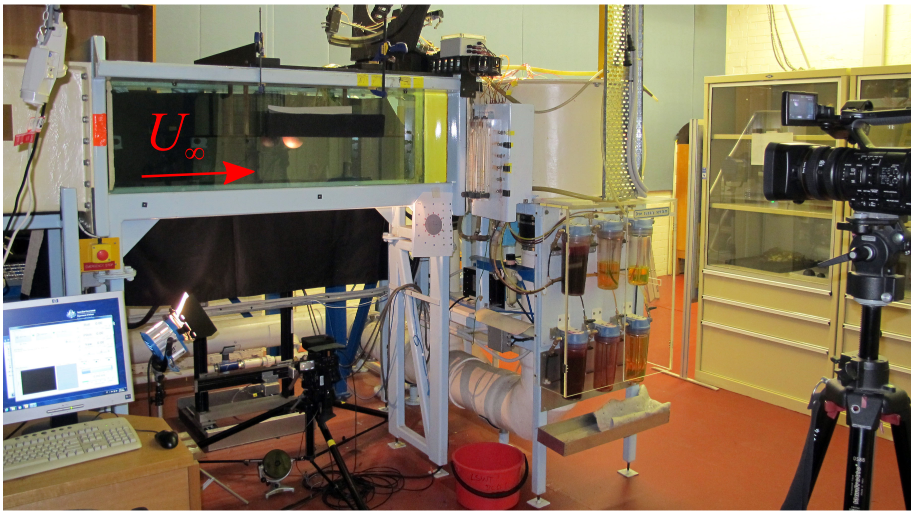

Figure 7: DST Water Tunnel with full experimental setup installed.

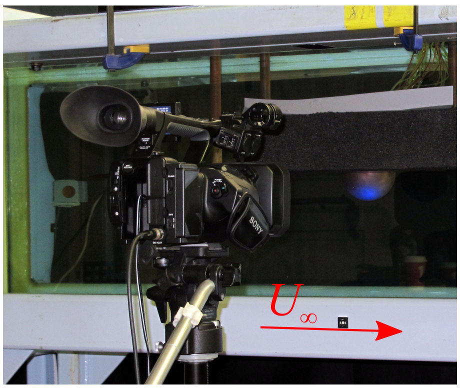

(i)

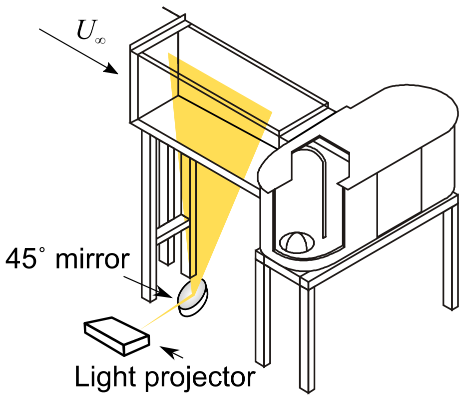

(ii)

Figure 8: DST Water Tunnel with (i) cross-section camera set up for capturing flow visualisations and (ii) the lighting setup schematic for the thin light sheet.

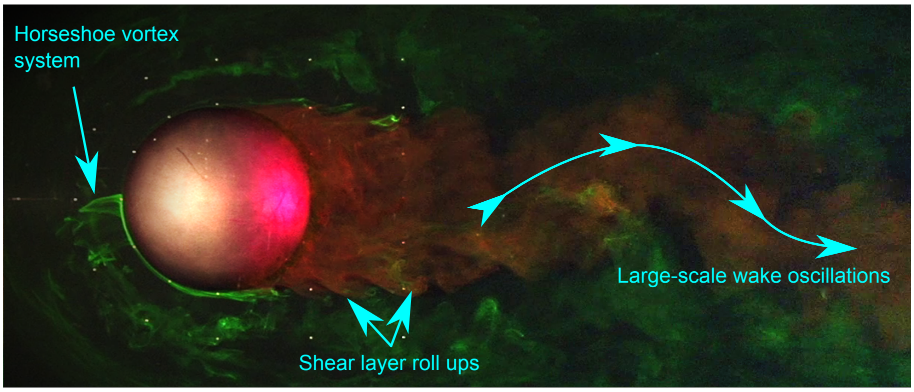

Figure 9: Overview of the flow around a hemisphere at $Re_D = 6.91 \times 10^3$ with some key visible flow structures highlighted.

3. Results and Discussion

Observations made in this study generally corroborated previous research. Key expected flow structures, such as the upstream horseshoe vortex system, recirculation zone, shear layer roll up and hairpin vortices were all visualised in the flow with varying degrees of clarity. The overall flow field, with some of the key flow structures highlighted, is shown in Fig. 9.

Each key flow structure deserves individual discussion. The horseshoe vortex system seemed complex with large spatio-temporal variation. The separated region and shear layer generally remained periodic, but the wake region was highly unsteady and could exhibit aperiodic behaviour. All of these regions and phenomena are discussed in the following sections, with particular emphasis on the unsteadiness of the flow field, which might contribute to unsteady loads on the hemisphere. It should be noted that in all images showing results, the free-stream flow direction is from left to right.

3.1. Horseshoe Vortex System

Using the light sheet configuration (Fig. 8), the horseshoe vortex system that formed immediately upstream of the hemisphere near the ground plane could be visualised. These vortices are characteristic of junction flows [16] and have also been observed extensively for surface mounted hemispheres. The observed behaviour of these vortices is also consistent with the findings of [3], who described the formation of multiple horseshoe vortices that intertwine as they advect around the hemisphere and downstream. The horseshoe vortex system observed is shown in Fig. 10, where dye is entrained into different sections of the vortex system across the three images. Oscillations in the flow means that with a constant dye injection rate, the dye is entrained in different vortices at different times. There is no particular order to the frames in Fig. 10; they are presented solely to gain a better understanding of the horseshoe vortex dynamics, and should not be interpreted as equally spaced time portraits.

The largest vortex [a] is located close to the hemisphere and forms as the vorticity in the boundary layer is concentrated at the upstream pole of the hemisphere. This primary vortex is accompanied by a hierarchy of smaller vortices of the same rotational sense further upstream

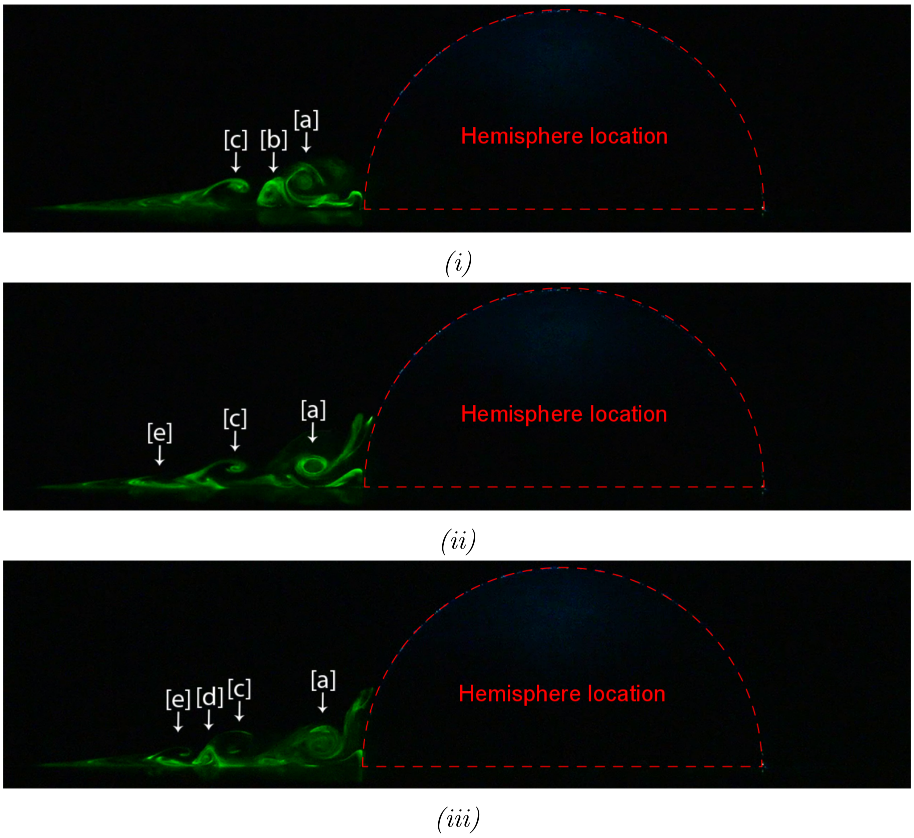

Figure 10: A series of frames taken during upstream centre-line injection showing the horseshoe vortex system at $Re_D = 6.91 \times 10^3$.

[c & e]. In between each successive pair there is a counter rotating induced vortex [b & d], and interactions between the vortices cause the entire system to oscillate in the stream-wise direction. At lower Reynolds number the dye became entrained into the horseshoe system much more effectively than at higher Reynolds number. The overall behaviour and development of multiple vortices did not seem to vary with Reynolds number, but the oscillations in the stream-wise direction became much more pronounced at $Re_D = 1.15 \times 10^4$. The extent to which the central focus of the primary horseshoe vortex moved in the stream-wise direction is highlighted in Fig. 11, where two images are overlaid and the upstream vortex location [u] colour is shifted to pink. The observed stream-wise distance between each position is approximately $x/D = 0.25$. This oscillatory behaviour is also illustrated in the two images shown in Fig. 12, where the dye injection rate and flow speed remain constant. By injecting dye at the upstream pole of the hemisphere (port S4), it was observed that the dye would alternate between becoming entrained into the horseshoe vortex and advecting directly around the sides and over the top of the hemisphere. This effect was significantly more pronounced at the higher Reynolds number. The dye also switched aperiodically between the $\pm y$ sides of the hemisphere when entrained in the horseshoe vortex; it may be seen in Fig. 12ii that there is more dye on the $-y$ side of the hemisphere at that instance in time.

A saddle point was observed by analysing the furthest upstream point marked by dye (Fig. 12ii). The horseshoe vortex system pushes dye away from the hemisphere and deposits it very close

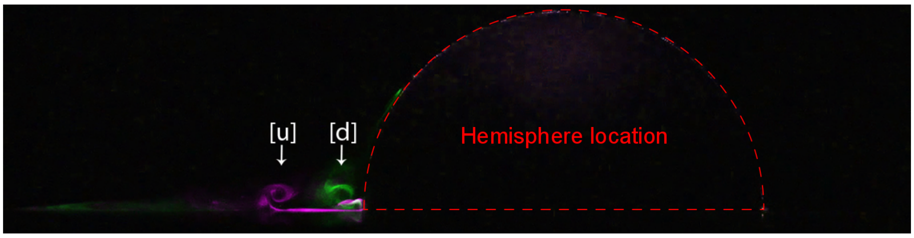

Figure 11: Oscillations in the primary horseshoe vortex observed at $Re_D = 1.15 \times 10^4$.

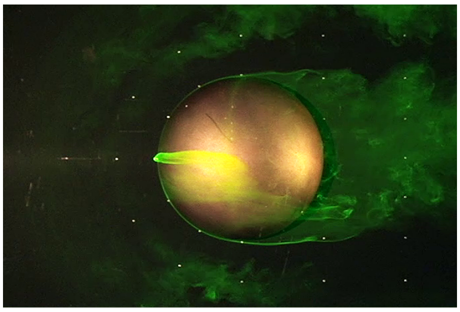

(i)

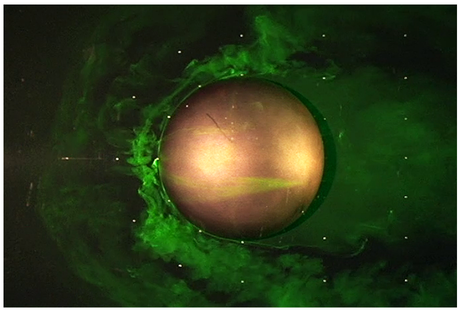

(ii)

Figure 12: Upstream centre-line injection at $Re_D = 1.15 \times 10^4$ *showing (i) flow around the hemisphere and (ii) entrainment in the horseshoe vortex system.*

to the ground plane, making the limiting streamlines visible at $x/D \approx -1.2$. This process shows a similar pattern to the computational results in [4], and the china clay surface visualisation reported by [13]. The large variation in Reynolds numbers between these studies indicates that this flow feature is persistent across a range of Re_D from 6,910 to over 150,000.

It is postulated that these stream-wise oscillations of the primary horseshoe vortex could contribute to unsteady motion of the stagnation point on the windward side of the hemisphere. When the primary horseshoe vortex core translates away from the hemisphere, it is probable that the resulting change in pressure distribution alters the streamlines and consequently the location of the stagnation point, but this requires further investigation.

3.2. Flow Attachment and Separation

Above the horseshoe vortex system the flow attaches to the hemisphere and accelerates through a favourable pressure gradient. The separation line on the hemisphere for both Reynolds numbers seemed to occur just prior to $\theta = 90°$, where θ is defined as per Fig. 13. No ground plane downstream reattachment point could be clearly discerned in the video footage, as the vortex structures in the wake diffused the dye quickly. Therefore, the change in recirculation zone size with Reynolds number, which infers a change in position of the reattachment point, was done by time averaging the video frames and applying a posterisation filter[2] in post processing (Fig. 14). This image processing method does not permit a quantitative assessment

[2]In image processing, posterisation algorithms de-construct the image colour data into a user-set discrete number of colours, which step change at the locations of maximum colour gradient in the original image, based on the number of discrete colours chosen.

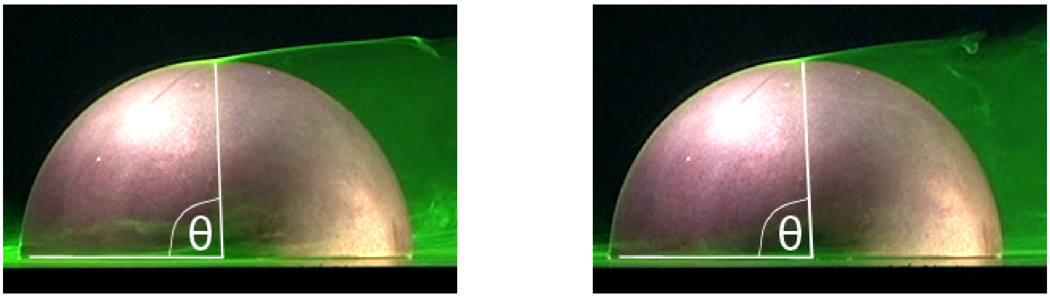

(i) *(ii)*

Figure 13: Hemisphere separation line at (i) $Re_D = 6.91 \times 10^3$ *and (ii)* $Re_D = 1.15 \times 10^4$.

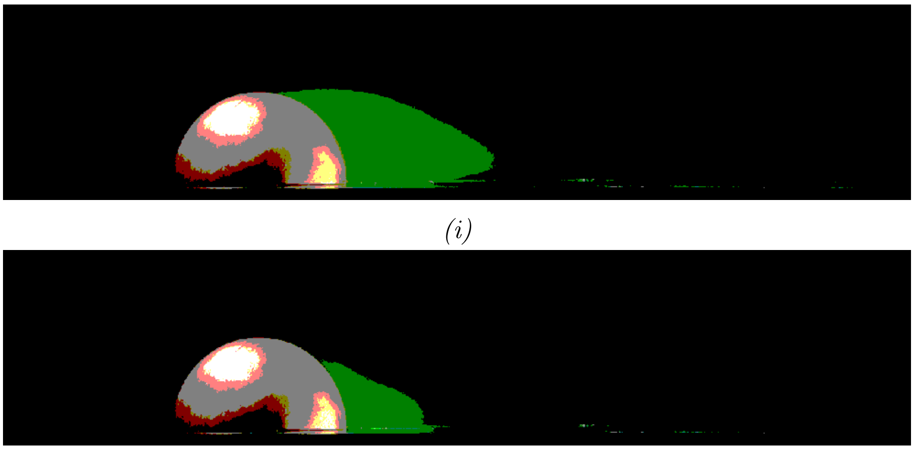

(i)

(ii)

Figure 14: Time-averaged, posterised images of the hemisphere recirculation zone at (i) $Re_D = 6.91 \times 10^3$ *and (ii)* $Re_D = 1.15 \times 10^4$.

of the recirculation zone size or variation, but with the constant lighting, dye injection rate and posterisation filter settings (varying the filter settings applied to both images did not affect the results), a qualitative observation of the variation in size can be made. The green shading in the hemisphere near wake is the time averaged region of dye recirculation, once the posterisation filter is applied. It can be seen that the recirculation zone size at $Re_D = 1.15 \times 10^4$ seems to have decreased relative to $Re_D = 6.91 \times 10^3$. This decrease in size with Reynolds number increase agrees with previous observations made by [3] and [13].

3.3. Shear Layer

The separated flow around the hemisphere forms a shear layer between the outer flow field and the recirculation zone in the hemisphere near wake. The planar view in Fig. 15 shows the shear layer formation in the wake. Here the dye has been injected along the streamwise centre-line at the hemisphere base (port S4); by injecting at a slightly higher flow rate, the dye momentum carries it past the horseshoe vortex system such that it advects over the hemisphere. The dye then enters the shear layer where it highlights the vorticity generation, and is eventually distributed through the vortex loop.

It was consistently observed that shear layer roll up would occur further downstream around the $\pm y$ sides of the hemisphere, such that the structure appears to be tilting upstream. This tilting is illustrated in the planar view in Fig. 15, where the two consecutive roll-ups are both curved such that the roll up over the top of the hemisphere [a] manifests further upstream than the roll up around the sides [b]. This sequence seemed to be periodic where the entire ring would appear, but with the difference in stream-wise location clearly evident. This tilting effect could be due to a number of factors including the interaction of the shear layer with the recirculation zone in the near wake, and a possible secondary interaction between the horseshoe vortex and the shear layer. Also visible in Fig. 15 is a coalescence of multiple roll-ups in the wake [c].

The pattern of shear layer roll up is dependent on Reynolds number. As previously described, the near-wake separated region is elongated at lower Reynolds numbers and there seemed to be a larger spatial distance between successive roll-ups. The shear layer roll-ups did not shed from the low pressure zone individually, rather successive roll-ups coalesced under mutual induction and formed the larger hairpin structures. In [5], the Strouhal number of both shear layer roll up and large-scale wake oscillations were calculated and a bifurcation at around $Re_D = 4,000$ was discovered – the higher St_D of which is related to the shear-layer vorticity and the lower to the large-scale wake oscillations (see Section 3.6). They concluded that this bifurcation was a direct result of coalescence of multiple shear layer roll-ups before shedding, which agrees with what was observed here. In fact, it appeared as though the coalescing of shear layer roll ups often preceded the detachment of hairpin vortices, and that mutual induction effects may play a part in determining the frequency of hairpin vortex shedding.

The approximate frequency of shear layer roll up was calculated by averaging the time taken for twenty consecutive vortex formations to pass a known stream-wise location. This process was repeated across a sample size of four separate image datasets. Using dye injection at ports F3-5 (Fig. 5) each roll up could be identified and visually counted. Results were calculated and averaged at each Reynolds number. The uncertainty in Strouhal number at 95% confidence was determined according to a 'Type A' assessment in [27], using a coverage factor of 3.18. The uncertainty was relatively high due to the subjectivity of the frequency calculation method, and small sample size. The results obtained here are overlaid on the results documented by [5] in Fig. 16, where the bifurcation at around $Re_D = 4,000$ may be clearly discerned. The shear layer roll-up Strouhal number calculated here for the lower Reynolds number case, $St_D = 1.7 \pm 0.14$, is in approximate agreement with the scatter data obtained by various methods of flow visualisation in [5], to within experimental uncertainty. In the higher Reynolds number case, the current results ($St_D = 2.4 \pm 0.22$) show a higher Strouhal number than the data in [5], but the reasons for this are currently unexplained.

3.4. Near-Wake Region

The near-wake region is characterised by the formation of a separated shear layer between the low pressure zone behind the hemisphere and the free-stream flow. The low pressure causes a significant back-flow, which was clearly observed in the direction of dye movement after injection into the near wake. On the stream-wise centre-line, the near-wake region oscillates between $\pm y$ as it is accelerated by the region of low pressure. This oscillation could be related to the large-scale wake oscillations explained in Section 3.6 and seems similar to a von Kármán

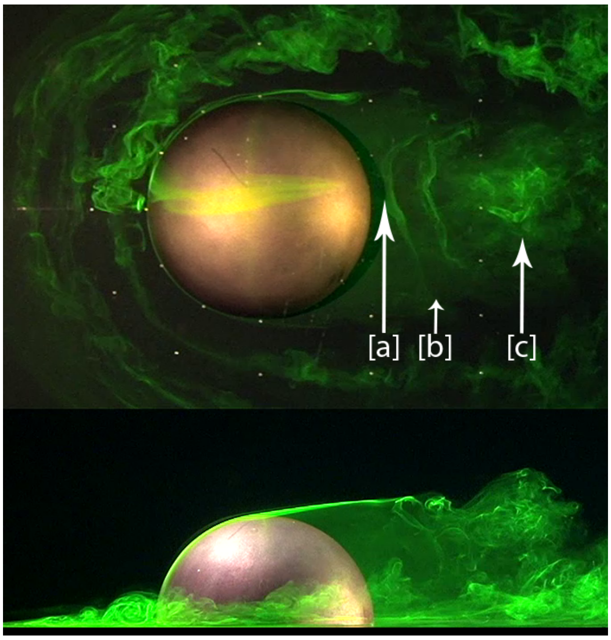

Figure 15: Shear layer roll up visualised in both planar (top) and cross-section (bottom) views at $Re_D = 6.91 \times 10^3$.

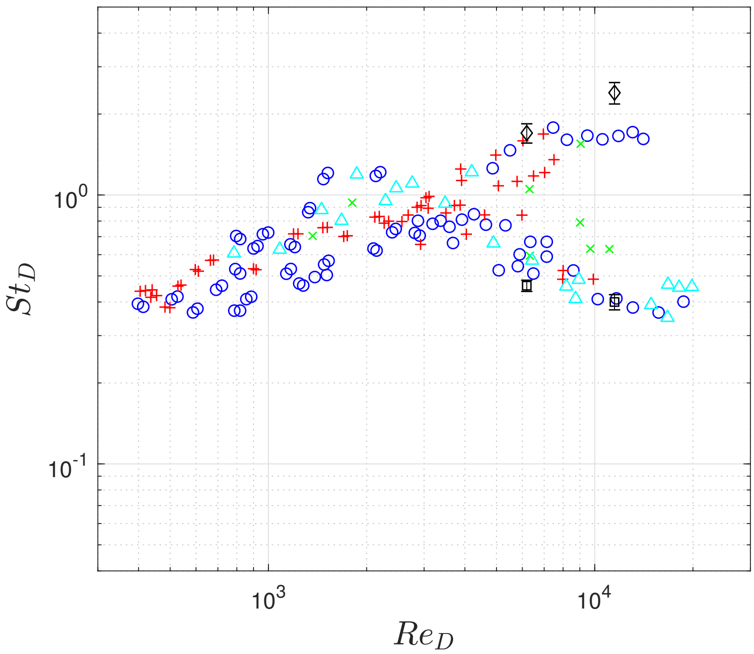

Figure 16: Comparison of (◇) shear-layer and (□) large-scale wake oscillation Strouhal numbers calculated here with uncertainty bars at 95% confidence against the data in [5]:(○) Aluminium particles, (+) Water blue dye, (×) Laser Doppler Anemometry and (△) Polyvinyl-Chloride particles.

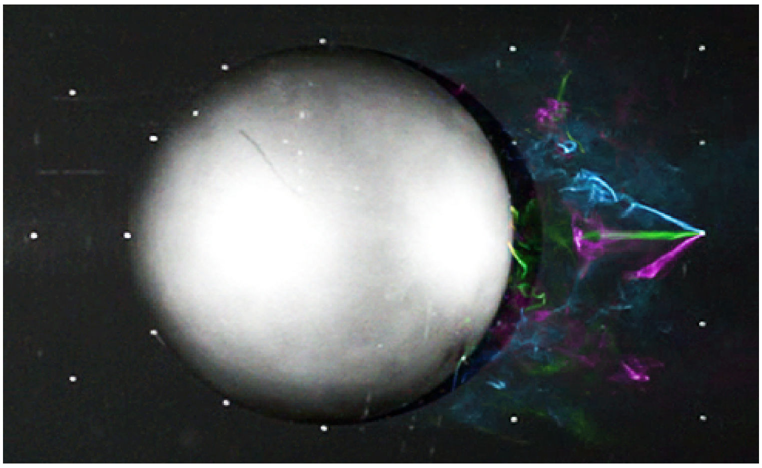

Figure 17: Overlay of three still images captured at $Re_D = 1.15\times10^4$ showing directly upstream flow (green), $-y$ angled flow (pink), and $+y$ angled flow (blue).

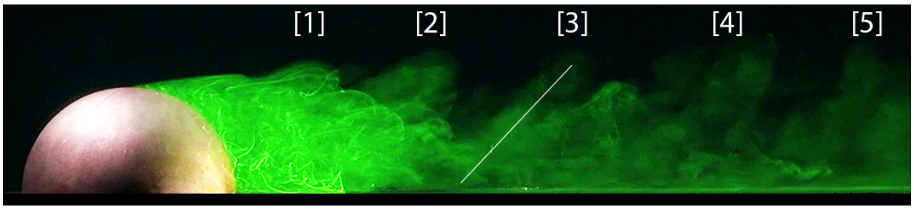

Figure 18: Hairpin vortices in the hemisphere wake at $Re_D = 6.91 \times 10^3$.

type anti-symmetric shedding. Oscillations about the stream-wise centre-line are visualised in Fig. 17 using injection port F4, where images are taken during one cycle and overlaid in different colours. Peak deflections observed sometimes exceeded those shown in Fig. 17 and the system did not always exhibit periodicity; at times, the dye seemed to meander randomly before settling back into a periodic motion. The magnitude of dye streamline deviation away from the x-axis was significantly greater for $Re_D = 6.91 \times 10^3$, with the flow even directed span-wise at times. This could be explained by the decreased reversed flow velocity also observed by [4, 13].

3.5. Far-Wake Region

Beyond the near-wake region the flow extends along the ground plane and exhibits coherent, large-scale vortical structures. After consecutive shear layer roll-ups have coalesced into hairpin vortices they advect downstream via the bulk fluid flow. An instantaneous time portrait captured during the shedding process at low Reynolds number is shown in Fig. 18. The heads of subsequent hairpins are visible and the shedding process is captured despite vorticity diffusing the dye. Each number in Fig. 18 corresponds to the head of an individual hairpin vortex, with the angled line qualitatively denoting vortex tilt angle. The observed behaviour of these hairpins is largely in agreement with [1]. As they advect downstream, vortex stretching distorts the hairpins such that the legs are further upstream than the head (see Fig. 1). This is most likely caused by the ground plane boundary layer; the heads of the hairpins are located in the free-stream flow, while the legs are located within the boundary layer. This hairpin

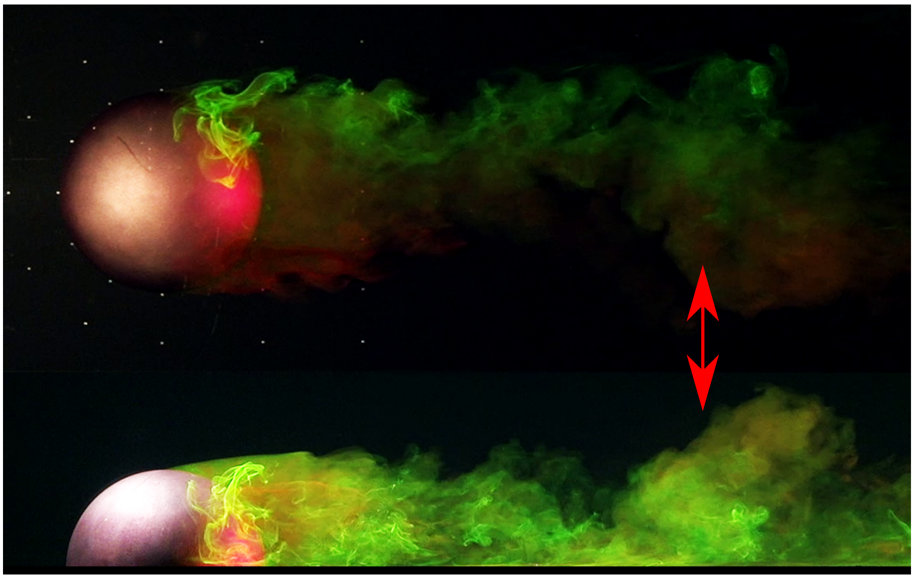

Figure 19: Coalescence of hairpin vortices, shown in both planar (top) and cross-section (bottom) views at $Re_D = 6.91 \times 10^3$.

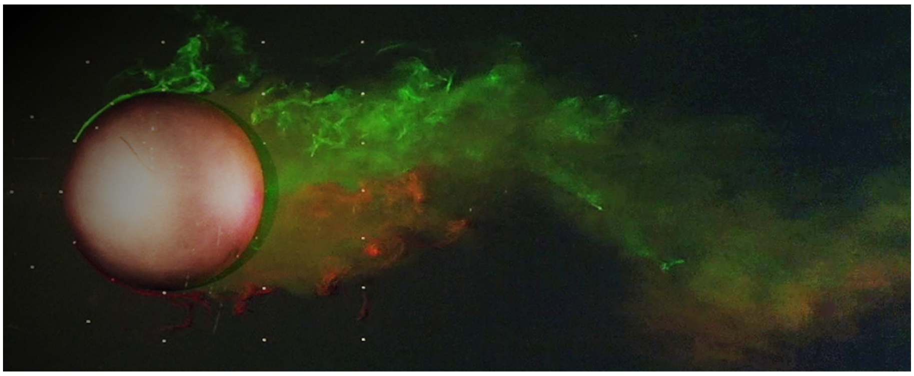

Figure 20: Planar footage of the large-scale wake oscillations at $Re_D = 1.15 \times 10^4$.

vortex tilt direction seems converse to the shear layer roll up tilt direction. Ostensibly, during coalescence and shedding, the head of each hairpin is accelerated past the legs.

It is important to note that the hairpin structures were not regularly visible during this experiment. It is unclear if this was to do with dye diffusing or simply not being entrained into the hairpins. There also exists the possibility that the hairpins themselves are not shed periodically. Contrary to the findings in [6], the hairpin vortices were observed to persist downstream past $x/D = 2$. In most cases, a hairpin vortex could be identified even past the elevated ground plane trailing edge (i.e. a length of $x/D = 5$).

3.6. Large-Scale Wake Behaviour

At both Reynolds numbers tested the entire wake oscillated about the stream-wise centreline (i.e. the $\pm y$ direction). As mentioned earlier, the pattern observed is similar to a von

Kármán anti-symmetric shedding type; however, the entire wake structure – including the hairpin vortices and the near-wake reversed flow region – oscillated. This phenomenon was more pronounced at the higher Reynolds number and is illustrated in Fig. 20. The frequency of these oscillations was approximated by recording the time taken for ten complete wake oscillations[3]. This process was repeated across a sample size of four separate image datasets, with uncertainty at 95% confidence in Strouhal number calculated identically to the shear layer roll-up results presented in Section 3.3. The data obtained here are also overlaid onto the results of [5] in Fig. 16.

The bifurcation in Strouhal number mentioned previously was described by [5] as 'formation' (shear layer roll-up) and 'shedding' (large-scale oscillations) of vortices, the latter of which exhibits a decreasing trend in Strouhal number as Reynolds number increases. This bifurcation has also been observed in this Reynolds number range for sphere wakes [28], and seems to appear in this study. It can be seen that at $Re_D = 6.91 \times 10^3$, the large-scale oscillations occur at $St_D = 0.46 \pm 0.02$ and decrease marginally to $St_D = 0.4 \pm 0.026$ at higher Reynolds number; there is good agreement within the bounds of data scatter with the observations in [5]. This agreement is interesting, given that the oncoming boundary layers were different in terms of state and thickness relative to the hemisphere. Additionally, there is evidence that the large-scale oscillation is also felt upstream of the hemisphere, as the horseshoe vortex system was observed to oscillate across the stream-wise centre-line. This is likely due to the time varying changes in circulation induced by the large-scale oscillations about the hemisphere base.

Occasionally the wake seemed to aperiodically form a much larger structure further downstream, which consisted of coalesced hairpin vortices (Fig. 19). Though not conclusive, it was interesting to note that the coalesced hairpin structures always formed at the maximum amplitude of the large-scale oscillations.

[3] In this study a complete wake oscillation frequency was defined as the time from one peak positive lateral excursion (such as that shown in Fig. 20) to the next positive peak in lateral excursion. In this period there are two large-scale shedding events. In contrast, the oscillation frequency defined in [5] appears to be based on shedding of discrete structures. Thus, the data here have been re-scaled by a factor of two to permit direct comparison.

4. Conclusions

A dye flow visualisation study on the flow-field surrounding a hemispherical protuberance has been undertaken. The aim of this research was to provide detailed imagery enabling further understanding of the flow structures around hemispherical protrusions, and the results presented here generally agree well with observations from previous studies. Some elements of the flow pattern were indicative of periodic processes, but many of the larger flow structures appeared aperiodic in nature and could not be easily attributed to known flow features. The present investigation has identified a number of additional behaviours not clearly explained in literature.

1. There are periodic oscillations of the primary horseshoe vortex core in the stream-wise direction not well described in previous flow visualisation studies. Limitations in the dye injection meant that estimating the frequency of this oscillation was not practical, but it is likely that this phenomenon influences the stagnation point location on the upstream pole of the hemisphere.

2. Large-scale wake oscillations were observed in the wake with a diameter based Strouhal number of around 0.4, which agrees with other studies. The Strouhal number of these oscillations seemed to show a marginal decrease as Reynolds number increased.

3. Coalescence of multiple shear layer roll-ups into hairpin vortices was observed to occur at higher Strouhal numbers than the large-scale wake oscillations, for a given Reynolds number. The Strouhal number of these structures seemed to increase as Reynolds number increased.

4. The horseshoe vortex system oscillated in the span-wise direction. This pattern seems to be related to the large-scale wake oscillations at a Strouhal numbers of around 0.4.

5. Recommendations

Further work is needed to clarify some of the new observations in this study. In particular, targeted measuring of the pressure distribution on the windward side of the hemisphere could be matched with flow visualisation to better understand the horseshoe vortex system. It is also worth investigating the correlation between the large-scale wake oscillations and dominant pressure fluctuations felt in the wake. However, a *time-resolved* spectral analysis method, such as the windowed Fourier transform or wavelet transform, should be used in future to study unsteady pressure measurements, given the aperiodicity (i.e. non-stationarity) of the flow structures. Also, a higher power light source for the flow cross-section images, such as a collimated Light Emitting Diode (LED) or a laser, should be used in future to illuminate the dye more effectively.

6. Acknowledgements

The authors would like to thank Mr Paul Jacquemin for his technical assistance with the design of the ground plane, and Mr Kevin Desmond for his assistance with the operation of the water tunnel. The authors also acknowledge the assistance provided by Mr Peter Manovski, on the editing of the video footage.

7. References

[1] Acarlar, M. S. & Smith, C. R. (1987) A study of hairpin vortices in a laminar boundary layer Part 1: Hairpin vortices generated by a hemisphere protuberance, *Journal of Fluid Mechanics* **175**, 1 – 41.

[2] Fedrezzi, M., Giacobello, M., Soria, J., Atkinson, C. & Jones, M. (2012) Experimental investigation of a hemisphere in a thin flat plate boundary layer, *in 18th Australasian Fluid Mechanics Conference*, Launceston, Australia.

[3] Savory, E. & Toy, N. (1986) The flow regime in the turbulent near wake of a hemisphere, *Experiments in Fluids* **4**(4), 181–188.

[4] Wood, J. N., De Nayer, G., Schmidt, S. & Breuer, M. (2016) Experimental investigation and large-eddy simulation of the turbulent flow past a smooth and rigid hemisphere, *Flow, Turbulence and Combustion* **97**(1), 79–119.

[5] Tamai, N., Asaeda, T. & Tanaka, N. (1987) Vortex structures around a hemispherical hump, *Boundary-Layer Meteorology* **39**(3), 301 – 314.

[6] Savory, E. & Toy, N. (1986) Hemispheres and hemisphere-cylinders in turbulent boundary layers, *Journal of Wind Engineering and Industrial Aerodynamics* **23**, 345 – 364.

[7] Achenbach, E. (1974) Vortex shedding from spheres, *Journal of Fluid Mechanics* **62**(2), 209 – 221.

[8] Kim, D. & Choi, H. (2003) Laminar flow past a hemisphere, *Physics of Fluids* **15**(8), 2457 – 2460.

[9] Taylor, T. (1991) Wind pressures on a hemispherical dome, *Journal of Wind Engineering and Industrial Aerodynamics* **40**(2), 199 – 213.

[10] Taniguchi, S. (1982) Time-averaged aerodynamic forces acting on a hemisphere immersed in a turbulent boundary layer, *Journal of Wind Engineering and Industrial Aerodynamics* **9**(3), 257 – 273.

[11] Cheng, C. & Fu, C. (2010) Characteristic of wind loads on a hemispherical dome in smooth flow and turbulent boundary layer flow, *Journal of Wind Engineering and Industrial Aerodynamics* **98**, 328 – 344.

[12] Almosnino, D. & McAlister, K. W. (1984) *Water-Tunnel Study of Transition Flow Around Circular Cylinders*, Technical report, NASA AMES Research Center, Moffett Field, California.

[13] McCarthy, J., Giacobello, M. & Lam, S. (2018) On the wavelet coherence of surface pressure fluctuations due to Von Kármán vortex shedding near a hemispherical protuberance, *Experiments in Fluids*. Under review.

[14] Okamoto, S. (1982) Turbulent shear flow behind hemisphere-cylinder placed on ground plane, *Turbulent Shear Flows* **3**, 171 – 185.

[15] Tang, Z. & Jiang, N. (2011) Dynamic mode decomposition of hairpin vortices generated by a hemisphere protuberance, *Science China Physics, Mechanics and Astronomy* **55**(1), 118 – 124.

[16] Simpson, R. L. (2001) Junction flows, *Annu. Rev. Fluid Mech.* (33), 415 – 443.

[17] Suzuki, Y. (1987) Pressure fluctuations on the surface of a hemisphere immersed in a thick turbulent boundary layer, *Journal of Fluids Engineering* **109**(2), 130 – 135.

[18] Zhou, Z., Wang, Z. & Fan, J. (2010) Direct numerical simulation of the transitional boundary-layer flow induced by an isolated hemispherical roughness element, *Computer Methods in Applied Mechanics and Engineering* **199**(23-24), 1573 – 1582.

[19] Manhart, M. (1998) Vortex shedding from a hemisphere in a turbulent boundary layer, *Theoretical and Computational Fluid Dynamics* **12**(1), 1–28.

[20] Tavakol, M., Yaghoubi, M. & Motlagh, M. M. (2010) Air flow aerodynamic on a wall-mounted hemisphere for various turbulent boundary layers, *Experimental Thermal and Fluid Science* **34**(5), 538 – 553.

[21] Gordeyev, S. & Jumper, E. (2010) Fluid dynamics and aero-optics of turrets, *Progress in Aerospace Sciences* **46**, 388 – 400.

[22] Erm, L. (2006) *Development of a Two-Component Strain-Gauge-Balance Load-Measurement System for the DSTO Water Tunnel*, Technical Report DSTO-TR-1835, Defence Science and Technology Organisation.

[23] Rolling Hills Research Corporation (2014) *Research Water Tunnels*.

[24] Smits, A. J. (2012) *Flow visualization: techniques and examples*, World Scientific.

[25] Barlow, J., Rae, W. & Pope, A. (1999) *Low-Speed Wind Tunnel Testing*, 3rd edn, John Wiley & Sons Inc., New York.

[26] Manovski, P., Giacobello, M. & Soria, J. (2007) Particle image velocimetry measurements over an aerodynamically open two-dimensional cavity, *in 16th Australasian Fluid*

Mechanics Conference, School of Engineering, University of Queensland.

[27] Cook, R. R. (2002) *Assessment of Uncertainties of Measurement*, 2nd edn, National Association of Testing Authorities.

[28] Kim, H. J. & Durbin, P. A. (1988) Observations of the frequencies in a sphere wake and of drag increase by acoustic excitation, *Physics of Fluids* **31**(11), 3260 – 3265.

DISTRIBUTION LIST

Flow Visualisation Around a Hemispherical Protuberance in the DST Group Water Tunnel

André Franck Bauer, Jesse McCarthy and Matteo Giacobello

Defence Science and Technology Group

Chief of Aerospace Division

Dr Greg Bain, RL AP&S

Mr Bruce Woodyatt, GL A&A

Dr Malcolm Jones, STL Experimental Aerodynamics

Dr Stephen Lam, S&T Manager Experimental Aerodynamics

Dr Matteo Giacobello, STL Computational Aerodynamics

Dr Jesse McCarthy

Mr André Bauer, Summer Vacation Program Scholar

DEFENCE SCIENCE AND TECHNOLOGY GROUP DOCUMENT CONTROL DATA				1. DLM/CAVEAT (OF DOCUMENT)
2. TITLE Flow Visualisation Around a Hemispherical Protuberance in the DST Group Water Tunnel		3. SECURITY CLASSIFICATION (FOR UNCLASSIFIED LIMITED RELEASE USE (L) NEXT TO DOCUMENT CLASSIFICATION) Document (U) Title (U) Abstract (U)		
4. AUTHORS André Franck Bauer, Jesse McCarthy and Matteo Giacobello		5. CORPORATE AUTHOR Defence Science and Technology Group 506 Lorimer St, Fishermans Bend, Victoria 3207, Australia		
6a. DST GROUP NUMBER DST-Group–TR–3482	6b. AR NUMBER 017-170	6c. TYPE OF REPORT Technical Report	7. DOCUMENT DATE April, 2018	
8. OBJECTIVE ID	9. TASK NUMBER	10. TASK SPONSOR		
11. MSTC Aircraft Performance and Survivability		12. STC Aerodynamics and Aeroelasticity		
13. DOWNGRADING/DELIMITING INSTRUCTIONS		14. RELEASE AUTHORITY Chief, Aerospace Division		

15. SECONDARY RELEASE STATEMENT OF THIS DOCUMENT

Approved for Public Release

OVERSEAS ENQUIRIES OUTSIDE STATED LIMITATIONS SHOULD BE REFERRED THROUGH DOCUMENT EXCHANGE, PO BOX 1500, EDINBURGH, SA 5111

16. DELIBERATE ANNOUNCEMENT

No Limitations

17. CITATION IN OTHER DOCUMENTS

No Limitations

18. RESEARCH LIBRARY THESAURUS

Flow visualisation, Water tunnel tests, Vortices, Video cameras

19. ABSTRACT

The flow structures around a hemispherical protuberance were studied using dye-injection flow visualisation in the DST Group Water Tunnel. A 100 mm diameter hemisphere was placed in a laminar oncoming boundary layer, and video imaging of the dye streamlines were captured at diameter-based Reynolds numbers of 6.91×10^3 and 1.15×10^4. The observations generally agree well with previous studies, while analysis of the video footage has provided additional insight into the evolution of the unsteady flow field.